Bulletin of the Seismological Society of America. Vol. 67, No. 2, pp. 301-313. April 1977

SOURCE PARAMETERS OF MODERATE SIZE EARTHQUAKES AND THE IMPORTANCE OF RECEIVER CRUSTAL STRUCTURE IN INTERPRETING OBSERVATIONS OF LOCAL EARTHQUAKES

By Donald V. Helmberger and Lane R. Johnson

ABSTRACT

Broadband observations of three central California earthquakes as recorded on opposite sides of the San Andreas fault zone are studied. The earthquake mechanisms are of the strike-slip type occurring along the fault at epicentral distances between 15 and 30 km. The seismograms obtained at the two sites are distinctly dissimilar in both amplitude and wave shape even though they are at roughly the same azimuth. We suppose that the earthquake excitation is identical for the two sites and that the differences in seismograms are caused by the receiver structure. The problem is idealized by assuming that the first 10 sec of each record can be modeled synthetically with a point shear dislocation embedded in a half-space with a two-layer upper-crustal model appropriate for each site. The results determined by matching the observations indicate that the durations for these events with M_L = 4 to 5 are about 0.3 to 0.6 sec. Furthermore, the results demonstrate that accurate estimates of source parameters can only be accomplished after a detailed appreciation of crustal structure.

Introduction

Recent demands for accurate scaling laws for various size earthquakes has greatly increased interest in local observations of moderate size events that are too small to be well recorded teleseismically but large enough not to be commonly included in aftershock sequences. Most attempts at extracting the source parameters from such local observations have used the corner-frequency approach where one makes no effort to separate source-generated effects from propagational effects introduced by local crustal structure but works with the spectral characteristics of the entire record, see for example Thatcher and Hanks (1973). While this approach has been significant in establishing the importance of duration or corner frequency in relation to the other source parameters, it has not resolved the meaning of the large scatter in stress drops due to the qualitative nature of the analysis.

Observations within a source depth of the event help to minimize propagational distortions; but separating near-field from far-field effects for an event that is not well located is extremely difficult (see Johnson and Helmberger, 1976). Also, it is not often that a moderate size event occurs directly under a broad-band instrument capable of remaining in operation. However, some exceptional observations as recorded by the San Andreas Geophysical Observatory (SAGO) in central California have been reported on recently by Johnson and McEvilly (1974). They were able to explain these broad-band observations at the smaller epicentral distances with simple point dislocation sources. At distances greater than about 15 km these observations begin to show considerable complexity and will be analyzed in more detail in this study.

The locations of the events relative to the two broad-band stations SAGO-Central and SAGO-East, are given in Figure 1. SAGO-E is situated near exposed Pliocene sedimentary rocks with outcrops of Franciscan to the northeast whereas SAGO-C is sitting on granitic rocks of the Gabilan range. The earthquakes farther to the south

are of the right-lateral transcurrent type with focal mechanism parameters given in Table 1, after Johnson and McEvilly (1974). The observations are displayed in Figure 2 where it is clear that the similarity of the various events at each station is far greater than the similarity of the same event at both stations. Note that the amplitudes are about a factor of two to three greater at SAGO-E as well. The three observations at SAGO-E are not only similar to each other but they also look much like the wave forms observed along a profile running parallel to the fault discussed by Helmberger and Malone (1975). These observations are displayed in Figure 3 along with synthetics generated for a layered model derived in that study. The agreement between the

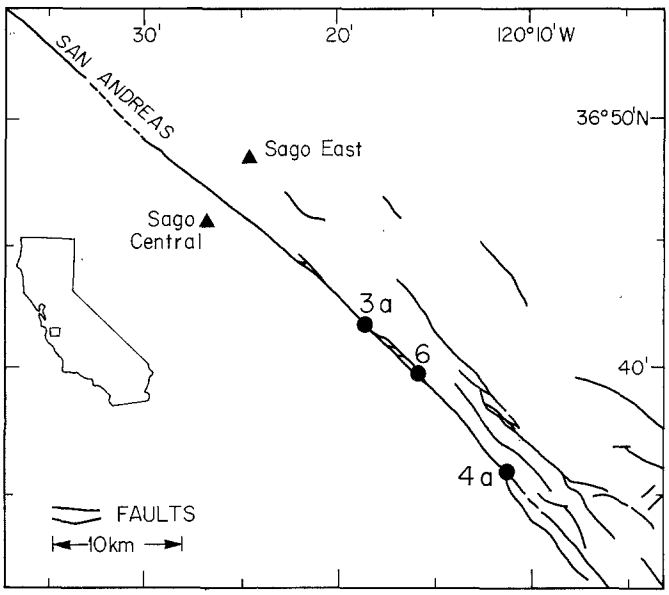

FIG. 1. A map of a section of the San Andreas fault in central California showing the locations of the seismographic stations SAGO-Central and SAGO-East relative to the three earthquakes studied. The identification numbers key the earthquakes to Table 1.

TABLE 1

DATA SUMMARY

Event No.	M_L	Depth (km)	SAGO-C		SAGO-E	
			Distance (km)	Azimuth (deg)	Distance (km)	Azimuth (deg)
3a	4.0	3.7	13.2	311	14.8	334
4a	5.1	6.4	29.7	311	30.7	322
6	4.7	5.1	21.3	310	22.4	325

synthetics and observed seismograms in the first 10 sec of motion is quite good, but thereafter the fit rapidly deteriorates. We interpret this phenomenon in terms of an imperfect surface wave guide that does not support the high degree of coherency necessary for the complete Love wave-train development. This interpretation can be examined in more detail by scrutinizing the actual construction of the synthetic for a simple one layer over a half-space model as displayed in Figure 4 where the index "n" is used to indicate the number of generalized rays used in the various stages of development. The top comparison includes only the direct generalized ray labeled

$n = 1$. The synthetic for the next comparison, $n = 2$, includes the first multiple reflection in the layer where the reflection point at the surface is slightly greater than 1.5 km from the receiver. The case of two multiples, $n = 2$, has two reflections at 3 km and 1.5 km, respectively, and as the number of reflections increase, more of the layer is involved in the propagation as the love wave begins to develop. Comparing the synthetic with the observation indicates that the fit is relatively good for about

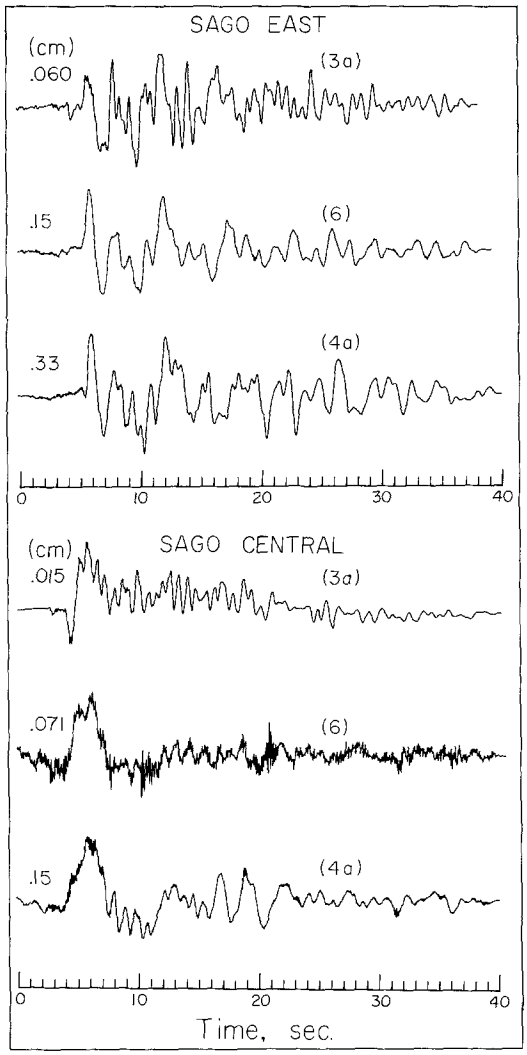

FIG. 2. The tangential displacement seismograms (SH-components) at SAGO-East (*top*) and SAGO-Central (*bottom*) for events (3a), (6) and (4a). The original NS and EW seismograms are displayed in Figures 19 and 20 of Johnson and McEvilly (1974).

the first 10 sec which are described by the first 4 or 5 rays, and thereafter the fit rapidly deteriorates. It thus appears that much of the complexity observed on local seismograms and their corresponding spectra can be explained in terms of upper crustal structure near the seismographic station. We investigate this hypothesis further in this paper where we will attempt to model the observations of Figure 2 synthetically.

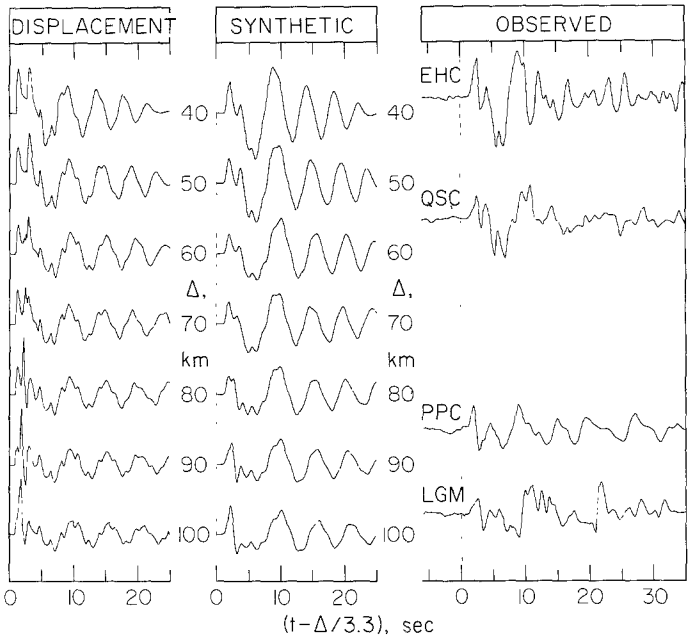

FIG. 3. Comparison of synthetics with observations with all traces plotted on the same amplitude scale. The moment is determined by overlay to be 2.1×10^{22} ergs.

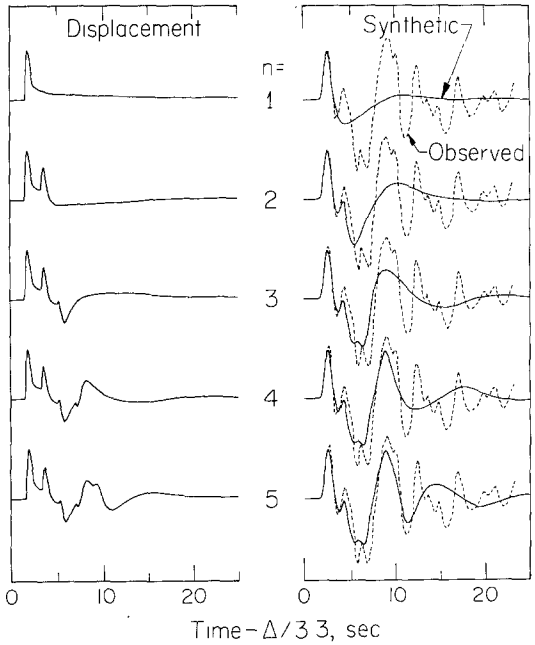

FIG. 4. Generation of synthetic response as a function of ray summation where the amplitudes are normalized to the *top trace*. The layer parameters are β = 1.5 km/sec and ρ = 2.0 gm/cm^3 with a thickness of 1.5 km. The half-space parameters are β = 3.3 km/sec and ρ = 2.6 gm/cm^3 and the source depth is 6 km.

ANALYSIS

The strategy used in the model determination was simply to match the first 10 sec of observations for one of the events with the fewest number of parameters (layers) and to predict the behaviors at the other two ranges. We assume that these strike-slip

earthquakes can be replaced by a point shear dislocation and the motion is controlled by pure *SH*-type motion at these azimuths. The matching procedure is basically a trial and error technique where a starting model is assumed. Next, the corresponding displacement for an assumed source excitation is constructed along with the synthetic seismogram. After comparing the synthetic with the observation in question and previous attempts, one makes the appropriate alterations in the model and repeats the process. Since we know more about the structure on the east from the previous study, we initiate the above procedure on SAGO-E at $\Delta = 30$ km.

Modeling SAGO-E. As a starting model we used model A proposed by Helmberger and Malone (1975) derived from observations obtained approximately 20 km to the

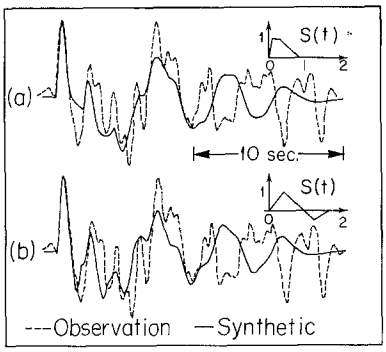

FIG. 5. Comparison of synthetics generated from the model A of Helmberger and Malone (1975) with SAGO-E for the (4a) event.

TABLE 2

UPPER-CRUSTAL MODELS

Model	Layer No.	Thickness (km)	Velocity (km/sec)	Density (gr/cm³)
E	1	0.35	0.75	1.5
	2	1.95	1.80	2.2
	3	∞	3.3	2.6
W	1	0.75	3.5	2.7
	2	1.75	2.7	2.6
	3	∞	2.0	2.6

east of the fault. Using the appropriate SAGO-E instrument response as described by Johnson and McEvilly (1974) one obtains the synthetics in Figure 5. We assumed a far-field source-time function, $F(t)$, of trapezoidal form described by δt_1, δt_2 and δt_3 as shown schematically in the right-hand corner of Figure 5a. The comparison with the observed record is made in overlay format. A reduction in the size of the first peak relative to later arrivals can be achieved by simply reducing the source depth but the overswing or the size of the first trough cannot be obtained so easily. Of course, this feature can be obtained by allowing the fault to overshoot producing a time function as shown in the right-hand corner of Figure 5b. This feature produces a possible solution but a simpler explanation is obtained by introducing a layer of low-velocity material (sediments) at the surface. These sediments are exposed along the eastern edge of the fault and are apparent as travel-time delays (Boore and Hill,

1973). With the addition of this low-velocity layer we have essentially four parameters to vary. After a diligent search we obtained model E given in Table 2 with corresponding step responses given in Figure 6. These results are similar to those presented in Helmberger and Malone (1975) at the longer periods but they have a strong 1-sec

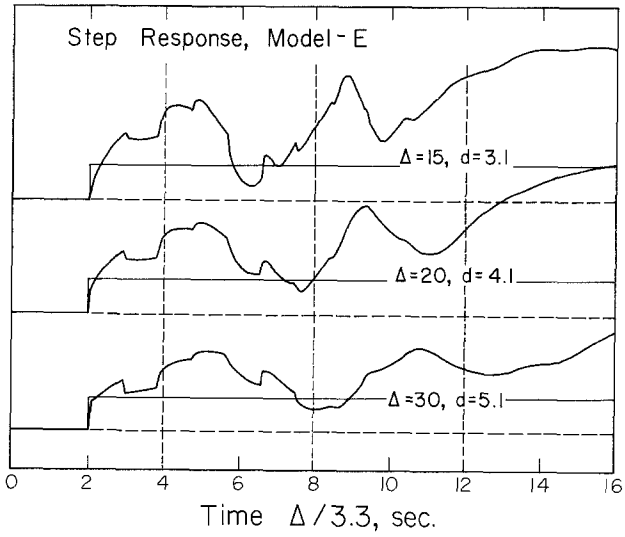

FIG. 6. Step-function responses as a function of range, Δ, and depth, d, for model E. The first-motion approximation to the far-field response (optics) appropriate for a half-space is included for comparison.

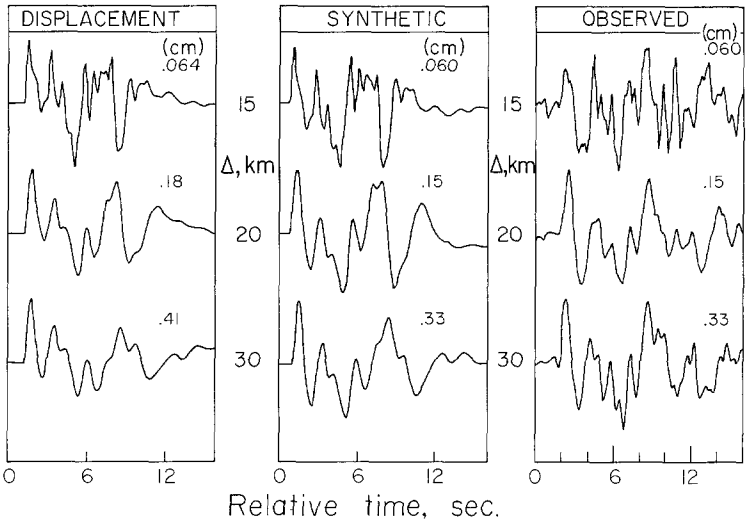

FIG. 7. Comparison of synthetics with observations at SAGO-E with the amplitudes given in centimeters. The source parameters used are given in Table 3.

periodicity produced by the soft superficial layer. The comparison of the corresponding synthetics with the SAGO-E observations is displayed in Figure 7. To reduce the number of parameters we assumed $\delta t_1 = \delta t_2 = \delta t_3 = \delta t$ and picked the best-fitting δt allowing δt to vary from 0.1 to 1. The moment is determined by scaling the synthetic to the corresponding observation. The results are given in Table 3. Note that we adjusted the depths somewhat, essentially making all three events shallower.

These changes are well within epicentral depth locations as determined from travel times and were done to produce the relative strengths of the first arrival to later arrivals. Changing the epicentral depth is quite effective for this purpose as discussed by Helmberger and Malone (1975).

Modeling SAGO-C. For the western model, we draw from two studies one by Mellman and Helmberger (1974) on diffraction effects caused by a high-velocity layer, the other by Boore and Hill (1973) who obtained a shear velocity of about 3.5 km/sec

TABLE 3

SOURCE PARAMETERS

Event No.	M_L	Moment (dyne-cm)	Source Duration (sec)
3a	4.0	1.6×10^{22}	0.3
4a	5.1	3.1×10^{23}	0.6
6	4.7	8.9×10^{22}	0.6

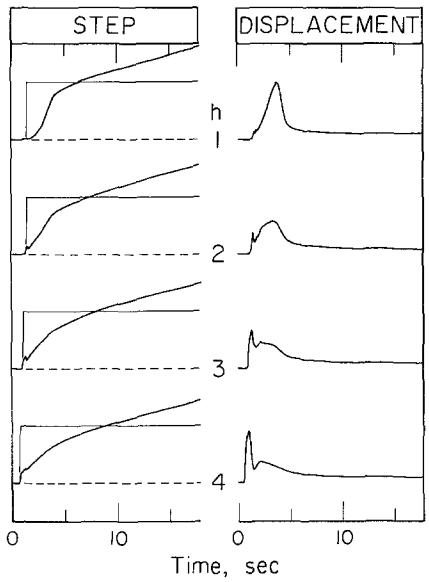

FIG. 8. Step and displacement responses for various layer thicknesses, h, at a range of 30 km with the strike-slip source at a depth of 6 km. The source duration parameters are $\delta t_1 = 0.1$, $\delta t_2 = 0.2$ and $\delta t_3 = 0.5$ sec.

for the granitic rocks. We thus assumed a layer ($\beta = 3.5$ km/sec) over a half-space ($\beta = 2.5$ km/sec) as a preliminary model to test for the effects diagnostic of a lower-velocity zone at depth. The results are displayed in Figure 8 where the responses are at the same range with the layer thickness as the only variable. Most of the short-period energy is reflected into the half-space when the layer is thin; that is the transmission coefficient for the direct ray (onset time) increases by over a factor of three going from $h = 1$ to 4 km. There is also considerable interference of the multiple reflections as is evident from the glichs near the beginning. In general, the polarity of these multiples will oscillate since the reflection coefficient is positive at the base of the layer. The large increase in amplitude a few seconds after the onset is essentially the direct arrival as h goes to zero. This effect is produced by the shape of the Cag-

niard contour as discussed by Helmberger and Malone (1975) and Mellman and Helmberger (1974).

Applying the experience learned from this example, we attempted to find a model that would produce the proper broadening of the first pulse that is so evident in Figure

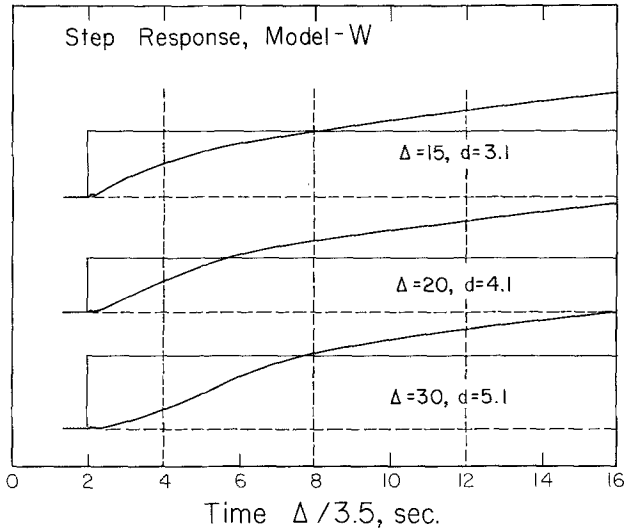

FIG. 9. Step-function responses as a function of range and depth for model *W*. The first-motion approximation of the far-field response for a half-space with model parameters appropriate for the bottom material is included for comparison.

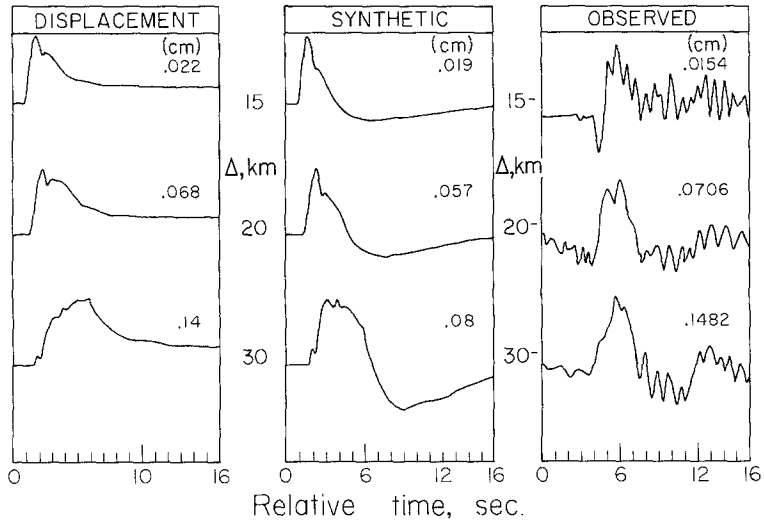

FIG. 10. Comparison of synthetics with observations at SAGO-C using the source parameter given in Table 3.

2. After investigating many two-layer models of various combinations of velocities we obtained model W given in Table 2 with the step responses and corresponding synthetics given in Figures 9 and 10. The amplitudes of the synthetics are appropriate for the moments as deduced from the SAGO-E observation and, in general, are somewhat too small at the larger ranges. Although the width of the positive pulses are about right at $\Delta = 15$ and 20 km, the synthetic at $\Delta = 30$ km is slightly too long and the backswings are obviously too long at all stations. However, it should be noted

that at these long periods we can no longer expect our earlier hypothesis about receiver structure to hold and that the entire path is now important, thus allowing lateral refractions along the fault to become a severe problem. The complexity of wave propagation in the three-dimensional structure that probably exists in this region is difficult to assess and thus our model must be viewed as speculative. However, it should be pointed out that if a direct high-velocity path existed between the source and receiver,

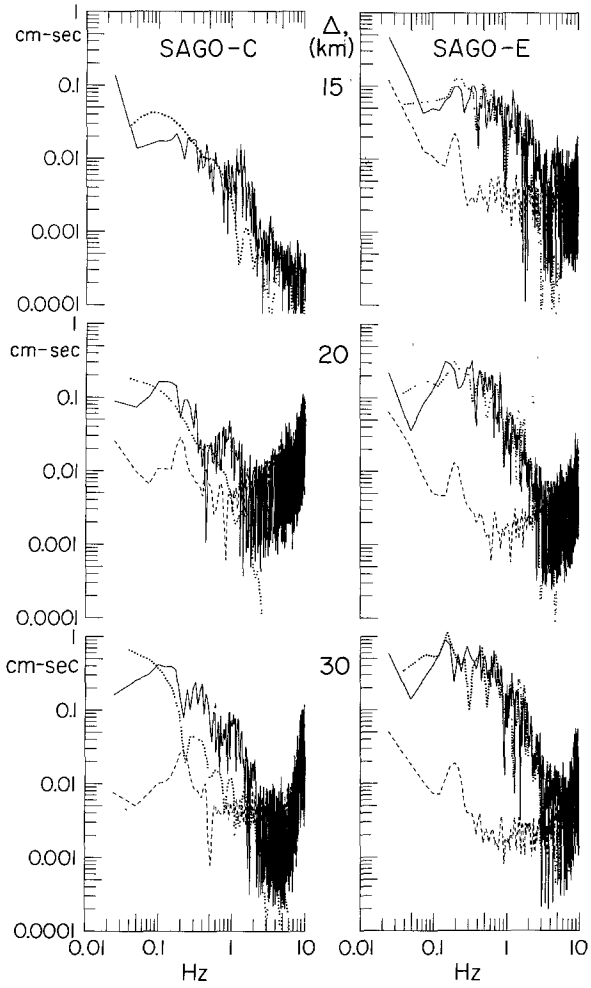

FIG. 11. Amplitude density spectra of the various events with the observed given as a solid line, synthetic by a dotted line, and estimates of the noise as a dashed line.

we would expect to see a sharp onset followed by an amplitude decrease caused by the loss of radiated energy into the low-velocity material on the other side of the fault zone. Thus, an alternative interpretation is that the faulting occurred on the northeastern side of a low-velocity zone associated with the San Andreas as proposed by Healy and Peake (1976), and this feature would essentially cut off the direct high-velocity path.

SPECTRA

The spectral comparison of the observations with synthetics is given in Figure 11. These spectra are based on the entire wave train and since the synthetics do not

contain the near-field terms we must be careful in our interpretation of the longer periods (Johnson and Helmberger, 1976). Furthermore, our models were determined by the early portion of recordings with a disregard of everything after 15 sec. Nevertheless, the agreement at SAGO-E is remarkably good with even some of the scalloping effects present although this is probably of minimal importance. One of the most important features of the observed spectra is the relative shift in peak values going from about 0.25 Hz at $\Delta = 15$ km to about 0.15 Hz at $\Delta = 30$ km. We interpret this effect as caused exclusively by the development of the surface waves which we feel is modeled quite well.

On the other hand, the agreement between observed and synthetic spectra at SAGO-C is not so good. The main problem is at the higher frequencies where the theoretical spectra fall off more rapidly than the observed, a fact which is also evident on the seismograms of Figure 10. This suggests that too much of a shadow-zone effect has been achieved in the synthetic calculations for SAGO-C, and that the low-velocity zone in model W is actually more extreme than necessary to match the observed seismograms.

It is worth noting that the general effect of a decay in the high-frequency energy which is achieved by the low-velocity zone in model W could also be achieved by introducing inelastic attenuation. Thus, another interpretation of the differences between SAGO-F and SAGO-C spectral data would postulate that the faulting occurs on the eastern side of a low-Q zone so that the high frequencies are more severely attenuated in propagating to SAGO-C. However, this interpretation will not explain the completely different wave shapes that were observed on the two sides of the fault at distances greater than 15 km.

Discussion

The observations examined in this study are probably too near the fault zone to obtain highly accurate estimates of the source parameters although SAGO-E seems explicable. Nevertheless, it is interesting to compare various size earthquakes that have been studied in the time domain with adequate corrections for earth structure. For convenience, we will define duration,

$$\tau = \tfrac{1}{2}\delta t_1 + \delta t_2 + \tfrac{1}{2}\delta t_3$$

and a corresponding corner frequency, $f_o = 1/(\pi\tau)$, after Helmberger and Malone (1975). The results, displayed in Figure 12, for the three events discussed earlier are supplemented by events 1, 2, and 7a modeled by Johnson and McEvilly (1974) and the Morgan Hill event studied by Helmberger and Malone (1975). At the larger magnitudes we included three events that have been modeled at teleseismic distances. These latter events have been modeled by inverting to long-period wave forms containing the main crustal phases P, pP, and sP and similarly for the S phases. The detailed information about fault orientation, depth, and source time duration are obtained by using the azimuthal coverage. Lines of constant stress drops are included for comparison although the actual level is rather arbitrary; that is, the stress drop is defined by

$$\Delta\sigma = (\tfrac{7}{16})M_o/r^3$$

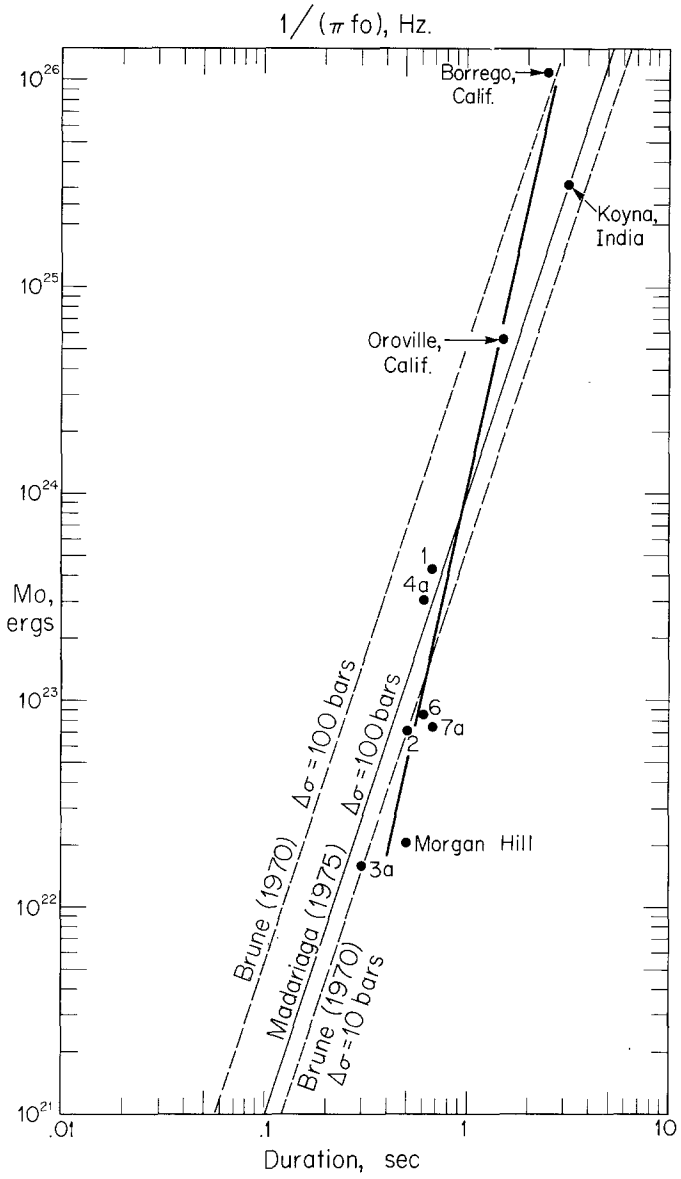

FIG. 12. Duration-versus-moment plot for the various events determined by fitting observations in the time domain. The data for the larger events are taken from Langston and Butler (1976) (Oroville), Langston (1976) (Koyna), and Burdick and Mellman (1976) (Borrego).

after Keilis-Borok (1959) for a circular fault surface with r = radius with estimates of

$$r = 3.5\,\beta/f_o \text{ (Brune, 1960)}$$

and

$$r = 0.21\,\beta/f_o \text{ (Madariaga, 1975).}$$

Accurate determinations of r independent of f_o have not been made although a number of experiments are presently designed for this purpose.

The trend of these points suggest that the larger events have higher stress drops than the smaller events at least for the California events, although the data selection may be biased in that the only broad-band data available in the $M_L = 4$ to 5 range comes from the Bear Valley region. It might also be argued that the Borrego and Oroville events may not be representative and that many more events must be considered before a definitive conclusion can be reached, especially events in the $M_L = 5.5$ range. The latter size is near the threshold of allowing body-wave studies at ranges 15° to 30° where the natural magnification caused by the upper mantle structure can be used to advantage; such studies are now in progress.

A meaningful relationship between duration versus moment is not only important with respect to learning something about stress changes in the Earth but it is essential to estimating strong ground motion for a given earthquake with a specified moment. We are suggesting that under ideal conditions ground motion amplitudes at periods 0.1 to 10 sec can be predicted if we know the source parameters, namely, moment, orientation, depth, and source duration, and if we know the receiver crustal response. The fault orientation and depth are of key importance in such predictions as demonstrated by Johnson and Helmberger (1976).

In summary, the broad direction of this paper has been to address the problem of separating effects due to structure as opposed to source by using recent developments in the methods of synthesizing motion in a layered half-space. Within this framework, a comparative analysis of the calculated and observed ground motions for several earthquakes was performed at two vastly different sites with respect to surface geology. Our results suggest that the beginning portion of local seismograms can be profoundly altered by the upper crustal structure. This means that the seismogram contains prominent periodicities, many of which are only weakly related to source radiation and, in fact, are more strongly related to the receiver structure. Once the receiver structure is known, or a transfer function determined which is a weaker condition, we come one step closer to estimating local ground motions for future events as well as learning something more about local geology.

Acknowledgments

This research was supported by the Advanced Research Projects Agency of the Department of Defense and was monitored by the Air Force Office of Scientific Research under Contracts F44620-72-C-0078 and F44620-72-C-0083 at the California Institute of Technology and AFOSR F44620-75-0049 at the University of California, Berkeley.

References

Boore, D. M. and D. P. Hill (1973). Wave propagation characteristics in the vicinity of the San Andreas fault, *Stanford Univ. Publ., Univ. Ser., Geol. Sci.* **13**, 214–223.

Brune, J. N. (1970). Tectonic stress and the spectra of seismic shear waves from earthquakes, *J. Geophys. Res.* **75**, 4997–5009.

Burdick, L. and G. Mellman (1976). Inversion of the body waves from the Borrego Mountain earthquake to the source mechanism, *Bull. Seism. Soc. Am.* **66**, 1485–1499.

Healy, J. H. and L. G. Peake (1975). Seismic velocity structure along a section of the San Andreas fault near Bear Valley, California, *Bull. Seism. Soc. Am.* **65**, 1177–1197.

Helmberger, D. V. (1974). Generalized ray theory for shear dislocation, *Bull. Seism. Soc. Am.* **62**, 561–589.

Helmberger, D. V. and S. D. Malone (1975). Modeling local earthquakes as shear dislocations in a layered half-space, *J. Geophys. Res.* **80**, 4881–4888.

Johnson, L. R. (1974). Green's functions for Lamb's problem, *Geophys. J.*, **37**, 99–131.

Johnson, L. and D. V. Helmberger (1976). The use of synthetic seismograms in interpreting observations from local earthquakes (in preparation).

Johnson, L. R. and T. V. McEvilly (1974). Near-field observations and source parameters of central California earthquakes, *Bull. Seism. Soc. Am.* **64,** 1855–1886.

Keilis-Borok, V. (1959). On estimation of the displacement in an earthquake source and of source dimensions, *Ann. Geofis., (Rome)* **12,** 205–214.

Langston, C. A. (1976). A body wave inversion of the Koyna, India, earthquake of 10 December 1967 and some implications for body wave focal mechanisms, *J. Geophys. Res.* (in press).

Langston, C. A. and R. Butler (1976). Focal mechanism of the August 1, 1975, Oroville earthquake, *Bull. Seism. Soc. Am.* **66,** 1111–1120.

Madariaga, R. (1976). Dynamics of an expanding circular fault, *Bull. Seism. Soc. Am.* **66,** 639–666.

Mellman, G. R. and D. V. Helmberger (1974). High-frequency attenuation by a thin high-velocity layer, *Bull. Seism. Soc. Am.* **64,** 1383–1388.

Thatcher, W. and T. C. Hanks (1973). Source parameters of southern California earthquakes. *J. Geophys. Res.* **78,** 8547–8576.

Division of Geological and Planetary Science
Seismological Laboratory
California Institute of Technology
Pasadena, California 91125 (D.V.H.)
Contribution No. 2738

Department of Geology and Geophysics
University of California
Berkeley, California 94720 (L.R.J.)

Manuscript received April 15, 1976